Fe(0) Nanoparticles for Nitrate Reduction: Stability, Reactivity, and Transformation

KYOUNGHEE SOHN,[†] SUNG WOOK KANG,[†]
SAMYOUNG AHN,*,[†]
MYUNGWU WOO,[‡] AND
SEONG-KOO YANG[§]

Departments of Environmental Education and Chemical Engineering, Sunchon National University, Sunchon, Jeonnam, 540-742, and The Center for Instrumental Analysis in Kyungnam University, Masan 631-701, Korea

The pyrophoric character of zerovalent iron nanoparticles and cumbersome handling of this material has been a drawback in practical applications, despite the expectation of an enhanced reactivity. We have been interested in how the iron nanoparticles can gain stability in air without significantly sacrificing reactivity. The freshly synthesized iron nanoparticles ignited spontaneously upon exposure to air. However, when exposed slowly to air, an ~5 nm coating of iron oxide was formed on the surface of particles. The oxide shell did not thicken for at least two months, indicating no sign of further corrosion of iron particles. The reactivity studies on nitrate reduction showed that the freshly synthesized iron reacted at the fastest rate. After formation of the oxide shell the rate constants decreased by ca. 50% of that of fresh iron, but were still higher than that of commercial grade micro- or milli-sized iron powder. Nitrate (50 ppm/350 mL) can be recharged 6 times into a bottle containing 0.5 g of iron nanoparticles. The reduction rate of the second cycle was the fastest among the six cycles, which can be attributed to the increase of surface area and the fresh iron surfaces that were bared by the dissolution of oxidized iron species on the surface. The oxidized iron was transformed to crystalline magnetite (Fe_3O_4) in solution.

Introduction

Recently, zerovalent iron has been intensively studied for the remediation of soil and groundwater contaminants such as chlorinated organic compounds (*1–3*), toxic metals (*4, 5*), and nitrate (*5–11*).

Due to the recent development of nanotechnology, researchers in environmental science have also shown interest in nanosized agents to improve the efficiency of chemical treatment to control contaminants. Nanosized zerovalent iron has shown an improved reactivity compared with micro- or milli-sized iron for the dechlorination of halogenated organic contaminants, and reduction of Cr(VI) and Pb(II) to Cr(III) and Pb(0) (*12–16*).

* Corresponding author e-mail: sahn@sunchon.ac.kr; phone: 82-61-750-3381; fax: 82-61-750-3308.
† Department of Environmental Education, Sunchon National University.
‡ Department of Chemical Engineering, Sunchon National University.
§ The Center for Instrumental Analysis in Kyungnam University.

Freshly synthesized iron nanoparticles often ignite spontaneously upon exposure to air or undergo a rapid exothermic reaction with oxygen under ambient aerobic conditions. TEM analyses of nanosized zerovalent iron reported in the literature have shown a core–shell structure with iron oxide surrounding the particles (*17–19*), and this oxide shell was claimed to protect the iron core from rapid oxidation in air. For reactivity studies using the zerovalent iron as a reagent to treat environmental pollutants, the oxide shell is an important factor in terms of stability to protect the inner iron and the ability to transport the charge and mass across it. Recently, Lowry et al. reported that the shell thickness could cause differences in reactivity of TCE dechlorination (*17*). However, there have been no systematic investigations as to how this oxide shell can be formed, how the aging of particles influences the shell thickness, whether the oxide shell gets thicker or alters their phase during reaction, and how the presence of the oxide shell affects the reactivity. In this study we explore the possibility that nanoparticles can be stabilized such that they can be handled in air in the absence of an inert gas environment and at the same time have reactivity superior to that of micro- or milli-sized iron on nitrate reduction. We have also investigated the physical characteristics of iron particles with different durations of exposure to air and studied how the aging process of iron influences its reactivity toward nitrate. XRD, TEM, and SEM were used to observe and quantify the particle morphology and oxidized iron precipitates during reduction.

Another important parameter to be considered for application of this technique is the efficiency of iron dose to reduce remediation cost. Reaction with zerovalent iron is heterogeneous, so iron concentration in the reactors was usually much larger than the stoichiometric requirement to complete the reduction (*5, 6, 9, 11, 20, 24, 25*). Therefore, unused iron particles remain after a treatment and it is worth estimating the efficient dose of iron for the reduction of a certain amount of nitrate.

Experimental Section

Preparation of Iron Nanoparticles. All procedures for syntheses and handling during this experiment were carried out under an atmosphere of N_2 (99.9%), using standard Schlenk and vacuum line techniques (*21*). All solvents were degassed and saturated with N_2 before use. Based on the literature (*16, 22*) iron nanoparticles were synthesized by adding KBH_4 solution to $FeSO_4 \cdot 7H_2O$ solution (mol ratio of $KBH_4/FeSO_4 \cdot 7H_2O = 2.5:1$). After addition of the KBH_4, the solution was stirred for 15 min under room temperature. The metal particles formed were settled, and the supernatant was decanted with a double-tipped needle. Then the solid was washed with degassed and deionized water several times and finally with degassed acetone. The resulting gray-black solid was vacuum-dried.

Formation of Thin Oxide Coating. A Schlenk flask containing freshly prepared iron nanoparticles was put into a desiccator. Then, the stopcock of the Schlenk flask was opened so that the nitrogen gas inside the flask and the air from outside gradually mixed and the iron nanoparticles slowly came into contact with air to form the protective iron oxide shell. Usually after 2 days iron nanoparticles could be handled in air.

Batch Experiments. Typically, a given amount of iron nanoparticles was charged into the Schlenk flask containing 350 mL of nitrate solution under stirring. The nitrate solution was deoxygenated by a N_2 stream for 2 h before adding iron. Periodically, 10 mL samples were withdrawn under a N_2
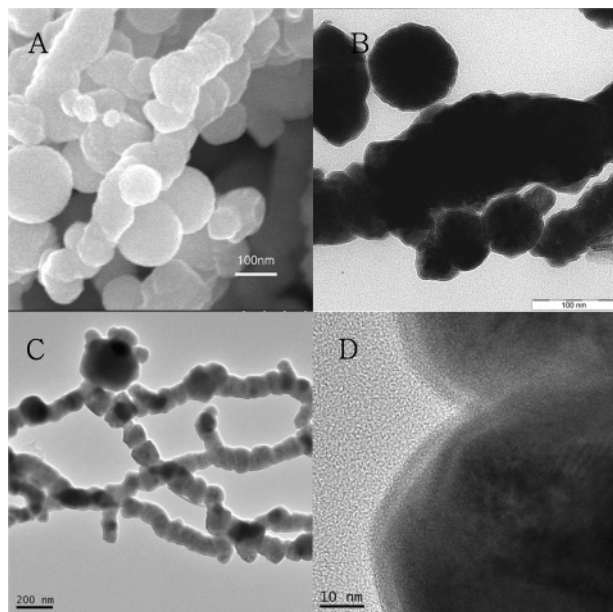
FIGURE 1. SEM and TEM images of iron nanoparticles: (A) SEM image; (B) TEM image of three-days aged particles; (C) HR-TEM image of two-months aged particles; (D) magnified HR-TEM image of two-months aged particles showing oxide coating.

FIGURE 2. X-ray powder diffraction patterns of the synthesized iron nanoparticles: (A) sample ignited spontaneously when freshly prepared iron was rapidly exposed to air; (B) three-days aged iron nanoparticles; (C) two-months aged iron nanoparticles.

stream and filtered through a 0.45 μm membrane filter (Advantec MFS). The concentrations of nitrate and nitrite were determined by ion chromatography (Dionex 120). Samples for the determination of ammonia were treated with a few drops of dilute HCl to trap ammonia as ammonium ion, which were then analyzed by ion chromatography or by UV (Shimadzu 1600) using the Indophenol method (*23*). The pH of the solution was not controlled.

Repetitive Reaction and Isolation of Iron Nanoparticles from each Cycle. Six reaction bottles were filled with a 50 ppm/350 mL nitrate solution and 0.5 g of iron. After the first round of reaction was performed, the iron particles were settled, and the solutions were decanted. Among six bottles, only one bottle was connected to a vacuum pump to dry the remaining solid. The other bottles were filled again with 50 ppm /350 mL of nitrate solutions and the reductions were performed. After the second round of reaction was complete, the iron particles were settled, and solutions were decanted. Among five bottles, one bottle was connected to the vacuum
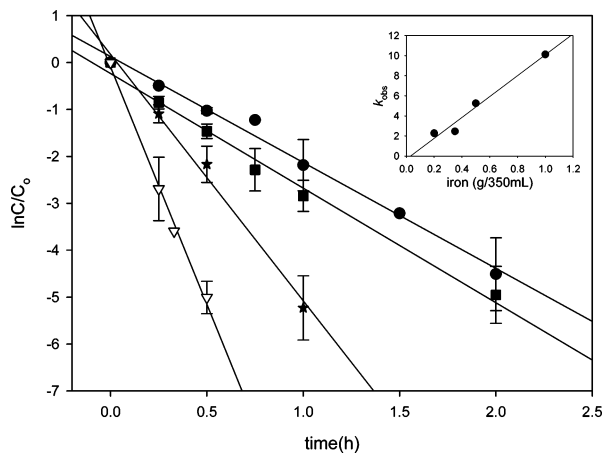
FIGURE 3. First-order kinetic for reduction of nitrate (50 ppm nitrate/ 350 mL). Variable: iron dosage; ● 0.2 g iron k_{obs} = 2.26 h⁻¹ (r^2 = 0.99), ■ 0.35 g iron k_{obs} = 2.44 h⁻¹ (r^2 = 0.98), ★ 0.5 g iron k_{obs}= 5.25 h⁻¹ (r^2 = 0.98), ▽ 1 g iron k_{obs}= 10.12 h⁻¹ (r^2 = 0.99). Inset: linear correlation between iron dose (g/350 mL) and k_{obs}.
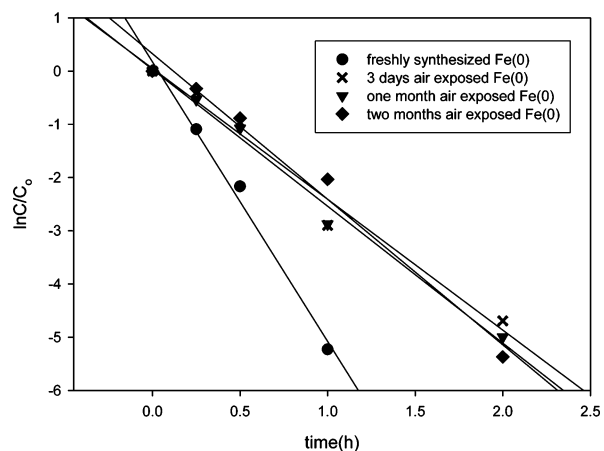
FIGURE 4. Aging effect of iron nanoparticles on the nitrate reactivity: ● freshly synthesized iron k_{obs}= 5.25 h⁻¹ (r^2 = 0.99); × three-days air exposed iron k_{obs}= 2.46 h⁻¹ (r^2 = 0.98); ▼ one-month air exposed iron k_{obs}= 2.57 h⁻¹ (r^2 = 0.98), ◆ two-months air exposed iron k_{obs}= 2.74 h⁻¹ (r^2 = 0.99).

pump to dry the remaining solid. The other four bottles were filled again with 50 ppm /350 mL of nitrate solutions and reductions were performed. This process was repeated until the sixth round of reaction was finished. Iron samples isolated from each cycle were exposed to air by the same method described above (Formation of Thin Oxide-Coating on Iron Nanoparticles) in order to be stabilized, and then were analyzed by SEM, TEM, and XRD.

Measurements. The surface area of the synthesized particles was measured using nitrogen adsorption method with a particle size analyzer (UPA-150, microtrac Korea basic science institute). XRD measurements were performed with the PW 1830 APD System (Panalytical, Netherland) equipped with a graphite monochromator (Cu Kα radiation, λ = 1.54056 Å), and qualitative analyses were achieved by an X'pert HighScore Plus (PW3121, Panalytical, Netherland) refinement program (Rietveld method). Surface morphologies of nano-particles were examined by a field emission scanning electron microscope (FE-SEM, Hitachi S-4700) operating at an ac-celeration voltage of 10 kV. The microscopic features of the sample were observed by a high-resolution transmission electron microscope (HR-TEM, JEM-2100F, JEOL, Japan, FRG-TEM) operating at 200 kV. Sample for TEM measurement were prepared on 200 mesh copper grid coated with carbon. After diluting the samples to an appropriate concentration

in ethanol, the solution was sonicated for 10 min, and then a copper grid was carefully dipped into the solution and dried under ambient temperature. The sample preparation for the measurements of XRD, TEM, and SEM was performed under atmospheric conditions without air protecting equipment. The pH was measured using HANNA instrument 8520.

Results and Discussion

Characterization of Iron Nanoparticles and Oxide Shell in Aging Processes. Morphology of the particles in diverse aging conditions was determined using SEM and TEM images, as shown in Figure 1. As described in the Experimental Section, the oxide coating was formed intentionally through gradual exposure of iron particles to air.

This oxide coating can be seen in Figure 1B and C as the slightly brighter shell surrounding the particles. The magnified high-resolution TEM in Figure 1D reveals that the oxide coating surrounds the large metallic cores with ca. 5 nm thickness. Figure 1C and D show two-months aged iron nanoparticles, indicating that the oxide shell, once it had been formed, did not thicken for at least two months. Tratnyek et al. (18) also observed the 5 nm thick oxide surrounding the iron core in TEM, even though they prepared the iron sample for TEM measurement in an anaerobic chamber. This indicates that surface iron was already oxidized before being mounted on the carbon-coated TEM grids. We also observed that occasionally the synthesized iron particles already had the oxide shell with same thickness, although not intentionally exposed to air. Combining our experience with the results of others, we can conclude that the oxide shell is formed during the synthesis procedure by casual contact with oxygen. In any case, whether it forms by intention or by accident, it obviously protects the inner zerovalent iron from further corrosion and is responsible for the stability of iron nanoparticles in air.

X-ray powder diffraction analyses (Figure 2) give supplementary information on the oxidation state of iron in diverse conditions. Figure 2A shows the formation of diverse phases of iron oxides after spontaneous ignition upon rapid exposure to air. Hematite and magnetite are the major oxide forms. Figure 2B shows the XRD pattern for iron nanoparticles that are gradually exposed to air. The sample was the same as that used in the TEM analysis of Figure 1B. Here, and also in the case of the two-months aged iron particles (Figure 2C), the signals of the iron oxide shell were not observed, possibly due to either amorphous phase of oxide or the diffraction was too weak. BET surface area analysis gave 8.1 ± 0.1 m^2/g (average of 2 measurements: 7.2 ± 0.1 and 9.0 ± 0.1 m^2/g). This value is lower than those previously reported (31.4−35 m^2/g) (14, 16, 17, 20), yet it is close to the BET value reported by another (5 m^2/g) under the same synthesis conditions (18). While specific surface areas (m^2/g) of iron nanoparticles are generally larger than that of micro- or milli-sized iron particles, they appear to have a large deviation depending on the synthesis method and conditions.

Reactivity of Nitrate Reduction: Nanosize Effect. Batch experiments were conducted to test the reactivity of fresh iron nanoparticles prepared in this way for nitrate reduction. Kinetic data were calculated from the average values of replicate tests ($n = 3−6$) for each set of reactions. Four different iron doses (0.2, 0.35, 0.5, and 1 g) with 50 ppm nitrate solution were tested. Nitrate removal rate fits the pseudo-first-order reaction kinetics very well (Figure 3). The observed rate constants (k_{obs}) of the freshly synthesized iron were 2.26 h^{-1} for 0.2 g of iron, 2.44 h^{-1} for 0.35 g of iron, 5.25 h^{-1} for 0.5 g of iron, and 10.12 h^{-1} for 1 g of iron. R^2 values ranged from 0.98 to 0.99. k_{obs} increased proportionally to the increasing amount of iron (r^2 is 0.98) under the tested reaction conditions (inset in Figure 3). Surface area normalized rate
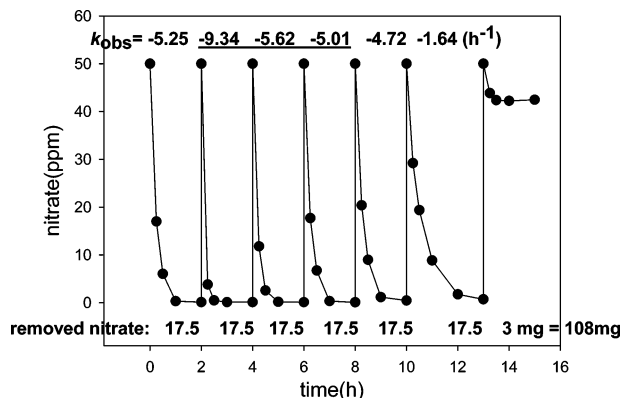
FIGURE 5. Repetitive reactions of 0.5 g of iron with nitrate; 350 mL of 50 ppm nitrate solution was repeatedly recharged. The rate constants: 1st, 5.25 h^{-1} ($r^2 = 0.99$); 2nd, 9.34 h^{-1} ($r^2 = 0.99$); 3rd, 5.62 h^{-1} ($r^2 = 0.99$); 4th, 5.01 h^{-1} ($r^2 = 0.99$); 5th, 4.72 h^{-1} ($r^2 = 0.99$); 6th, 1.64 h^{-1} ($r^2 = 0.99$).

constants, k_{SA}, were 0.42, 0.302, 0.45, and 0.44 L·m^{-2}·h^{-1}, respectively (average of 0.403 L·m^{-2}·h^{-1}).

For the purpose of comparison, the kinetic data obtained from other studies with micro- or milli-sized iron powders and our own experiment are summarized in Table S1 (Supporting Information). Mass normalized rate constants (k_m, L·g^{-1}·h^{-1}) and surface area normalized rate constant (k_{SA}, L·m^{-2}·h^{-1}) were calculated. Table S1 shows that both k_m and k_{SA} are larger with nanosized iron than micro- or milli-sized iron despite the different experimental conditions, which means that the enhanced reactivity with nanosized iron seems to be a general phenomenon.

In these experiments, pH increased rapidly to 9−10 within a few minutes after the beginning of the reaction and remained between 9.0 and 10 throughout the reaction, regardless of the amount of iron. The fact that nitrate was reduced so rapidly in the alkaline solution is very surprising, because nitrate reduction with micro- or milli-sized iron powders did not take place in alkaline solution above pH 9 or at least the reactivity decreased significantly. The optimum pH was reported to be weakly acidic (5, 9, 11, 24, 25). More detailed investigation is needed to determine the factors that drive the reduction of nitrate despite unfavorable pH. However, this finding has a very practical meaning because it is unnecessary to add an acid to reaction media continuously or to use a buffer solution in order to hold the pH of the solution to acidic condition.

Influence of Aging of Iron Nanoparticles on Nitrate Reduction. As shown above, freshly synthesized nanosized zerovalent iron shows superior performance for nitrate reduction, and the slowly air-exposed iron nanoparticles do not undergo a rapid oxidation in air (increased stability) due to the oxide shell. From a practical point of view, stability and reactivity are both important requirements for materials to treat environmental problems. To investigate the influence of aging of iron nanoparticles (thus, the influence of the oxide shell) on reactivity, we tested four types of iron nanoparticles: freshly synthesized iron, 3 days air-exposed iron, 1 month air-exposed iron, and 2 months air-exposed iron. All iron samples originated from a single batch, with aging as the only variable.

Figure 4 shows that k_{obs} of freshly synthesized iron was 5.25 h^{-1} (50 ppm/350 mL nitrate solution with 0.5 g of iron), and k_{obs} of aged iron nanoparticles decreased almost 50% resulting in 2.46 h^{-1} for 3 days aged iron, 2.57 h^{-1} for 1 month aged iron, and 2.74 h^{-1} for 2 months aged iron. These kinetic data show that iron nanoparticles with the oxide shell (aged one) sacrificed some reactivity compared to fresh iron, and once the oxide shell had been formed, there was no significant
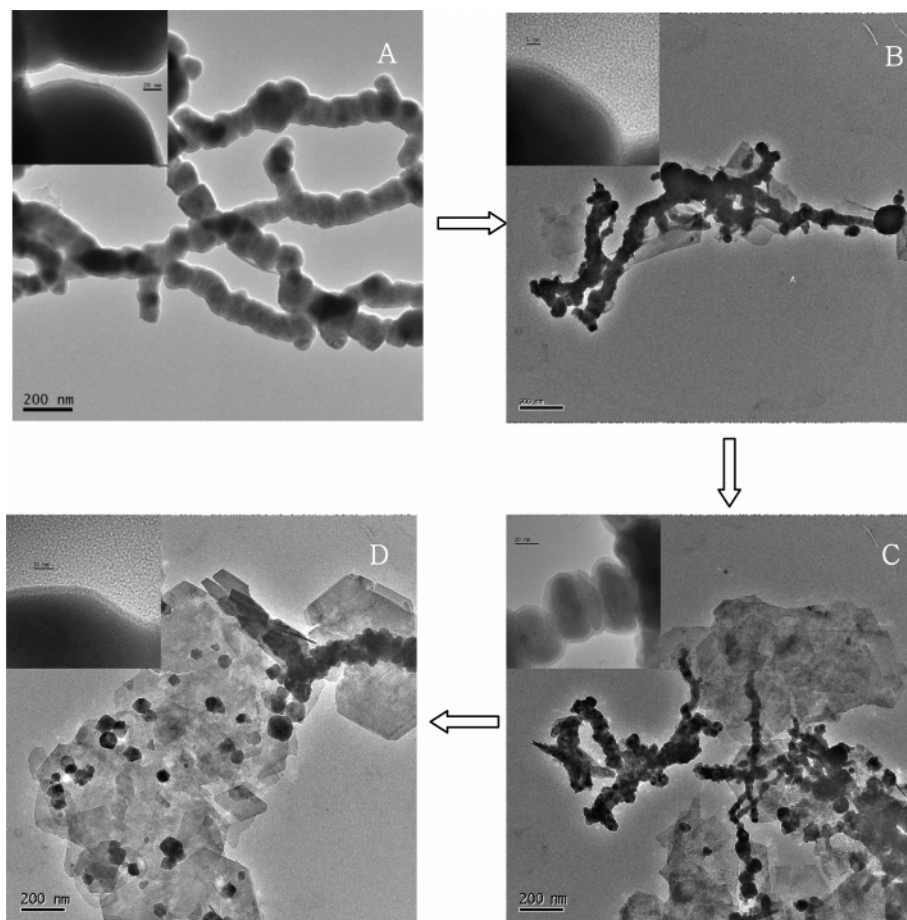
FIGURE 6. TEM images of the transformation of Fe(0) to magnetite during the repetitive nitrate reduction: (A) before the reaction; (B) after first reaction; (C) after third reaction; (D) after sixth reaction. Insets: HR-TEM images of iron nanoparticles showing ca. 5 nm thick iron oxide shell.

altering of reactivity during the tested periods. The air-exposed nanosized iron, with average $k_{obs} = 2.59$ h^{-1}, $k_m = 1.81$ L·g^{-1}·h^{-1}, and $k_{SA} = 0.22$ L·m^{-2}·h^{-1} still reduced nitrate much faster than micro- or milli-sized iron.

Therefore, iron nanoparticles used in our study seem to fulfill our expectation of dual benefits: stability in air and superior performance as a reducing agent for nitrate reduction. However, our result with the 5 nm thick oxide shell is limited to the experimental conditions tested. A further study is needed to elucidate whether the size of iron particle has an influence on the thickness of the oxide coating and thereby whether their thickness affects the reactivity.

Repetition of Nitrate Reduction and Transformation of Iron. Since the reduction occurs on the surface of iron, an excess of iron is usually employed. For an example in our experiment, 0.5 g (8.9 mmol) of iron was used to treat 50 ppm/350 mL (0.28 mmol) nitrate; this iron dose corresponds to 8-times excess (eq 1).

There has been no reference to the optimal amount of iron to reduce a certain quantity of nitrate while minimizing the loss of unused iron. To estimate the amount of iron needed, we carried out the following experiment: 50 ppm/350 mL nitrate solution was spiked repeatedly in a bottle containing 0.5 g iron until the reduction did not take place any more.

$$NO_3^- + 4Fe(0) + 10H^+ \rightarrow NH_4^+ + 4Fe^{2+} + 3H_2O \quad (1)$$
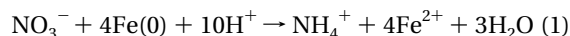
According to eq 1, 0.5 g of iron (8.93 mmol) can theoretically reduce 140 mg (2.23 mmol) of nitrate, assuming that all the iron is consumed as if the reaction occurred in a homogeneous condition. The result summarized in Figure 5 was very

astonishing. The reduction was repeated 6 times (theoretically 8 times, as the mass of nitrate in 350 mL solution is 17.5 mg (0.28 mmol)) and the amount of consumed iron reached 77% of the amount added. Furthermore, the rate of the second reaction ($k_{obs} = 9.34$ h^{-1}) was faster than the first, and even the third and fourth reaction rates (5.62 h^{-1} ($r^2 = 0.99$) and 5.01 h^{-1} ($r^2 = 0.99$)) were almost the same as the first.

There was speculation that the oxidized iron forms an insoluble oxide layer that will get thicker as the reduction proceeds (*26*). Then, the penetration of nitrate ions into the iron core becomes difficult and iron particles will be deactivated with a certain thickness of oxide layer (Scheme S1a). If this hypothesis were correct, we would expect a gradual decrease of reactivity as the reaction steps were repeated, and the reduction would take place only as long as charge and mass transfer through this oxide shell are possible. However, it turned out that the iron oxide layer did not thicken. Lowry et al. (*17*) also reported that they could not observe the growth of the oxide shell.

The HR-TEM of iron nanoparticles isolated after each repetitive reduction showed the ca. 5 nm thickness of oxide shell, almost the same thickness as the original nanoparticles before reaction (Insets in Figure 6). When dry iron particles isolated after the first, second, and third reaction were exposed to air without the pretreatment step of oxide formation (described in Experimental Section), they ignited spontaneously. This indicates that during reduction of nitrate the iron surface was peeled to bare the naked zerovalent iron surface. What may happen on the surface of the iron is proposed in Scheme S1b. As reduction takes place on the iron surface, the pH of the solution increases above 9 within
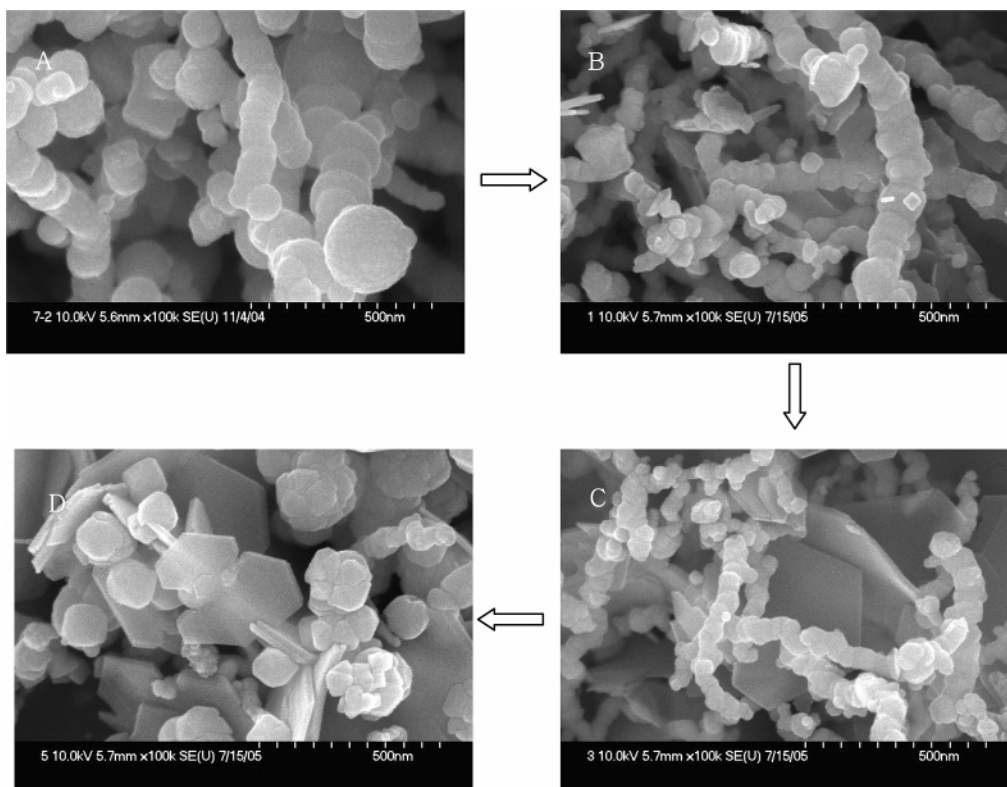
FIGURE 7. SEM images of the transformation of Fe(0) to magnetite during the repetitive nitrate reduction: (A) before the reaction; (B) after the first reaction; (C) after the third reaction; (D) after the sixth reaction.

a few minutes. In this basic condition the oxidized iron forms anionic hydroxo species, such as $Fe(OH)_y^{2-y}$ and $Fe(OH)_x^{3-x}$. These species are known to be soluble and unstable in alkaline media, so that they transform to another phase of iron oxide by reconstructive transformation mechanisms: dissolution and reprecipitation. The dissolution of oxidized iron offers fresh iron surface to nitrate ion resulting in an increase of reduction rate. The mechanical abrasion of oxides from the iron surface during mixing could be considered for peeling of the oxide shell, but it cannot explain the formation of the crystalline hexagonal plates of iron oxide shown in Figures 6 and 7. Therefore, this possibility seems to be very low.

TEM and SEM in Figure 6 and Figure 7 clearly show the transformation process of zerovalent iron to iron oxide. As the reduction was repeated, the size of zerovalent iron particles became smaller and a new compound in a hexagonal plate shape appeared (Figure 6). SEM in Figure 7 also showed the successive transformation of iron with the appearance of new species in a plate shape among zerovalent iron particles (TEM and SEM images of samples from the second and fourth reaction are given in Supporting Information, Figure S1 and Figure S2).

XRD analyses for samples from the repetitive reactions (Figure S3, Supporting Information) show the signals of zerovalent iron and magnetite (Fe_3O_4). Signal intensity of iron oxide increases and that of zerovalent iron decreases. The absence of two signals at $2\theta = 23.84$ ($hkl = 210$) and 26.19 ($hkl = 213$) excludes the possibility for iron oxide to be maghemite (γ-Fe_2O_3); except for these two signals, other XRD patterns of maghemite and magnetite are identical. Comparison of d spacing values of the formed iron oxide with standard JCPDS γ-Fe_2O_3 and Fe_3O_4 data are also in agreement with magnetite (Fe_3O_4) (Table S2, Supporting Information) (*27*). Under the highly reducing and alkaline conditions, magnetite is thermodynamically stable and major species (*27, 28*). Figure S4 shows the result of quantitative XRD analysis on the repetitive reaction, demonstrating that

the amount of iron oxide increased linearly in proportion to the number of reaction turns.

Of particular note is that specific surface area of the solid changed after the reduction. Specific surface area of the particles after the first reaction was 23.5 ± 0.4 m^2/g, after the second reaction was 25.4 ± 0.4 m^2/g, and after the third reaction was 27.2 ± 0.4 m^2/g. These values are approximately three times higher than that of iron nanoparticles before reaction. A necklace-like aggregate of iron nanoparticles may be disaggregated into a shorter chain by the corrosion of the surface iron. Newly formed iron oxide also contributes to specific surface areas and their portion will increase as the reaction is repeated, and the available iron diminished significantly at the fourth, fifth, and sixth reactions. Therefore, further investigation will be necessary to determine whether it is related to the enhanced rate constants, especially at the second and third reaction steps.

Nitrogen mass balance, defined as the percentage of the sum of measured NO_3^-, NO_2^-, and NH_4^+ over initial NO_3^-, was in the range of 80−90%. Presumably, the equilibrium between ammonium ion and ammonia shifts to ammonia due to the increase in pH of the solution in an alkaline range during the reaction, and ammonia can partially dissipate along with N_2 upon opening the reactor for sampling. A small amount of NO_2^- (below 1 ppm) as an intermediate was also detected (*6, 10, 11, 24*).

This work represents the first systematic effort to quantify the reactivity and the efficiency of nitrate reduction by iron nanoparticles, including their effect of aging on the reactivity and transformation pathway. Results from this study will enhance the application of nanosized iron and further the understanding of zerovalent iron in remediation processes.

Acknowledgments

Supporting Information Available

TEM and SEM images showing the successive transformation of iron to iron oxide, XRD of iron samples isolated from the repetitive nitrate reduction, a plot of the amount of iron oxide versus the number of repetition, a table showing the comparison of the reactivity of micro- or milli-sized iron and nanosized iron, a table showing the comparison of d spacing values of the obtained iron oxide with standard JCPDS γ-Fe_2O_3 and Fe_3O_4 data, a scheme showing proposed mechanism for the transformation of Fe(0) to magnetite during nitrate reduction. This material is available free of charge via the Internet at http://pubs.acs.org.

Literature Cited

(1) Matheson, J. L.; Tratnyek, P. G. Reductive dehalogenation of chlorinated methanes by iron metal. *Environ. Sci. Technol.* **1994**, *28*, 2045−2053.

(2) Johnson, T. L.; Scherer, M. M.; Tratnyek, P. G. Kinetics of halogenated organic compound degradation by iron metal. *Environ. Sci. Technol.* **1996**, *30*, 2634−2640.

(3) Eykholt, G. R.; Davenport, D. T. Dechlorination of the chloro-acetaniline herbicides alachlor and metolachlor by iron metal. *Environ. Sci. Technol.* **1998**, *32*, 1482−1487.

(4) Melitas, N. Wang, J. Conklin, M.; O'Day, P.; Farrell, J. Understanding soluble arsenate removal kinetics by zerovalent iron media. *Environ. Sci. Technol.* **2002**, *36*, 2074−2081.

(5) Alowitz, M. J.; Scherer, M. M. Kinetics of nitrate, nitrite, and Cr(VI) reduction by iron metal. *Environ. Sci. Technol.* **2002**, *36*, 299−306.

(6) Sianta, D. P.; Schreier, C. G.; Chou, C. S.; Reinhard, M. Treatment of 1,2-dibromo-3-chloropropane and nitrate-contaminated water with zerovalent iron or hydrogen/palladium catalysts. *Water Res.* **1996**, *30*, 2315−2322.

(7) Till, B. A.; Weathers, L. I.; Alverez, P. J. J. Fe(0)-supported autotrophic denitrification. *Environ. Sci. Technol.* **1998**, *32*, 634−639.

(8) Devlin, J. F.; Eedy, R.; Butler, B. J. Effect of electron donor and granular iron on nitrate transformation rates in sediments from a municipal water supply aquifer. *J. Contam. Hydrol.* **2000**, *46*, 81−97.

(9) Miehr, R.; Tratnyek. M. M.; Bandstra, J. Z.; Scherer, M. M.; Alowitz, M. J.; Bylaska, E. J. Diversity of contaminant reduction reactions by zerovalent iron: role of the reductate. *Environ. Sci. Technol.* **2004**, *38*, 139−147.

(10) Su, C.; Puls, R. W. Nitrate reduction by zerovalent iron: Effects of formate, oxalate, citrate, chloride, sulfate, borate, and phosphate. *Environ. Sci. Technol.* **2004**, *38*, 2715−2720.

(11) Huang, C. P.; Wang, H. W.; Chiu, P. C. Nitrate reduction by metallic iron. *Water Res.* **1998**, *32*, 2257−2264.

(12) Lien, H.-L.; Zhang, W.-X. Transformation of chlorinated methanes by nanoscale iron particles. *J. Environ. Eng.* **1999**, *125*, 1042−1047.

(13) Ponder, S. M.; Darab, J. G.; Mallouk, T. E. Remediation of Cr(VI) and Pb(II) aqueous solutions using supported, nanoscale zerovalent iron. *Environ. Sci. Technol.* **2000**, *4*, 2564−2569.

(14) Lien, H.-L.; Zhang, W.-X. Nanoscale iron particles for complete reduction of chlorinated ethens. *Colloids Surf., A* **2001**, *191*, 97−105.

(15) Li, F.; Vipulanandan, C.; Mohanty, K. K. Microemulsion and solution approaches to nanoparticle iron production for degradation of trichloroethylene. *Colloids Surf., A* **2003**, *223*, 103−112.

(16) Wang, C.-B.; Zhang, W.-X. Synthesizing nanoscale iron particles for rapid and complete dechlorination of TCE and PCBs. *Environ. Sci. Technol.* **1997**, *31*, 2154−2156.

(17) Liu, Y.; Majetich, S. A.; Tilton, R. D.; Sholl, D. S.; Lowry, G. V. TCE dechlorination rates, pathways, and efficiency of nanoscale iron particles with different properties. *Environ. Sci. Technol.* **2005**, *39*, 1338−1345.

(18) Nurmi, J. T.; Tratnyek, P. G.; Sarathy, V.; Baer, D. R.; Amonette, J. E.; Pecher, K.; Wang, C.; Linehan, J. C.; Matson, D. W.; Penn, J. C.; Driessen, M. D. Characterization and properties of metallic iron nanoparticles: spectroscopy, electrochemistry, and kinetics. *Environ. Sci. Technol.* **2005**, *39*, 1221−1230.

(19) Carpenter, E. E.; Calvin, S.; Stroud, R. M.; Harris, V. G. Passivated iron as core−shell nanoparticles. *Chem. Mater.* **2003**, *15*, 3245−3246.

(20) Choe, S.; Chang, Y.-Y.; Hwang, K.-Y.; Khim, J. Kinetics of reductive denitrification by nanoscale zerovalent iron. *Chemosphere* **2000**, *41*, 1307−1311.

(21) Shriver, D. F.; Drezdon, M. A. *The Manipulation of Air-Sensitive Compounds*, 2nd ed; Wiley: New York, 1986.

(22) Glavee, G. N.; Klabunde, K. J.; Sorensen, C. M.; Hadjipanayis, G. C. Chemistry of borohydride reduction of iron(II) and iron (III) ions in aqueous and nonaqueous media. Formation of nanoscale Fe, FeB, and Fe_2B powders. *Inorg. Chem.* **1995**, *34*, 28−35.

(23) Clesceri, L. S.; Greenberg, A. E.; Eaton, A. D. *Standard Methods for the Examination of Water and Wastewater*, 20th ed.; American Public Health Association: Washington, DC, 1998; pp 4−108.

(24) Ahn, S.; Oh, J.; Sohn, K. Mechanistic aspects of nitrate reduction by Fe(0) in water. *J. Kor. Chem. Soc.* **2001**, *45*, 395−398.

(25) Zawaideh, L. L.; Zhang, T. C. The effect of pH and addition of an organic buffer (HEPES) on nitrate transformation in Fe^0-water systems. *Water Sci. Technol.* **1998**, *38*, 107−115.

(26) Farrell, J.; Kason, M.; Melitas, N.; Li, T. Investigation of the long-term performance of zerovalent iron for reductive dechlorination of trichloroethylene. *Environ. Sci. Technol.* **2000**, *34*, 514−521.

(27) Cornell, R. M.; Schwertmann, U. *The Iron Oxides*; VCH: New York, 1996; p 166.

(28) Cornell, R. M.; Schwertmann, U. *The Iron Oxides*; VCH: New York, 1996; p 314.